Fluid Flow Programming in Paper-Derived Silica-Polymer Hybrids

*Christelle Dubois[1], Nicole Herzog[1], Christian Rüttiger[1], Andreas Geißler[1], Eléonor Grange[1], Ulrike Kunz[2], Hans-Joachim Kleebe[2], Markus Biesalski[1], Tobias Meckel[1], Torsten Gutmann[3], Markus Gallei[1], Annette Andrieu-Brunsen[1]**

[1]Ernst-Berl Institut für Technische und Makromolekulare Chemie, Technische Universität Darmstadt, Alarich-Weiss-Str. 4, D-64287 Darmstadt, Germany.

[2]Institut für Angewandte Geowissenschaften, Fachgebiet Geomaterialwissenschaft, Technische Universität Darmstadt, Schnittspahnstr. 9, D-64287 Darmstadt, Germany.

[3] Eduard-Zintl Institute for Inorganic and Physical Chemistry, Technical University Darmstadt, Alarich-Weiss-Str. 8, D-64287 Darmstadt, Germany.

Corresponding author: brunsen@cellulose.tu-darmstadt.de

KEYWORDS: mesoporous silica hybrid paper, sol-gel chemistry, redox-gating, capillary fluid flow, paper-based microfluidic devices.

ABSTRACT: In paper-based devices, capillary fluid flow is based on length-scale selective functional control within a hierarchical porous system. The fluid flow can be tuned by altering the paper preparation process, which controls parameters such as the paper grammage. Interestingly, the fiber morphology and nanoporosity are often neglected. In this work, porous voids are incorporated into paper by the combination of dense or mesoporous ceramic silica coatings with hierarchically porous Cotton Linter paper. Varying the silica coating leads to significant changes in the fluid flow characteristics, up to the complete water exclusion without any further fiber surface hydrophobization, providing new approaches to control fluid flow. Additionally, functionalization with redox-responsive polymers leads to reversible, dynamic gating of fluid flow in these hybrid paper materials, demonstrating the potential of length scale specific, dynamic, and external transport control.

INTRODUCTION

Microscopically and nanoscopically hierarchical porous structures with tunable fluid flow on very different length scales are interesting regarding their single molecule passage control. In this context, the casparian strip in combination with membrane proteins proves to be a fascinating example, achieving molecular control over the uptake of solved molecules.[1] Paper has the potential to mimic such complex fluid flow control if the function of different porous

length scales can be well-controlled, and further offers numerous advantages being a sustainable, low-cost, and disposable material. In order to achieve this, new approaches are needed to selectively introduce and functionalize different porous spaces.

Microfluidic paper-based devices have been investigated for manifold applications since their introduction by Whitesides.[2-3] To-date, the modulation of flow in paper-based materials has been investigated in terms of paper homogeneity and density, fluid viscosity, environmental conditions, and channel dimensions.[4-12] In particular, engineering the paper sheet morphology by altering the fiber source or the density of the paper sheet, or the "paper grammage", has recently been reported to accurately control the flow velocity.[4] Fluid penetration is typically prevented by rendering certain areas hydrophobic.[13] In a recent publication by Vlessidis and co-workers, channels were introduced parallel to the flow direction in order to accelerate the flow, whilst perpendicular channels caused the fluid flow to slow down.[14] Recently, inkjet printing has been proposed as a simple way to upscale paper-based devices.[15] Once materials are deposited into the paper sheet at the surface of the ligno-cellulosic fibers the mechanical properties, as well as the fluid imbibition by capillary forces, are affected.[16] With this in mind, if fluid flow modulation is to be precisely controlled, the influence of the fiber morphology must be better understood.

Moreover, in addition to adjusting the fluid velocity in paper, it would be advantageous to be capable of externally and dynamically manipulating the fluid flow e.g., by modulating the hydrophobicity, and thus the fluid-surface interactions. Responsive materials that display switchable surface wetting have been used in the preparation of self-cleaning surfaces, tunable optical lenses, lab-on-chip systems, microfluidic devices, textile applications, thin film sensors, and *smart* membranes.[17-25] In this context, ferrocene-containing polymers have shown great potential on planar surfaces and in mesopores.[21, 26] Regarding molecular passage control, functionalized mesoporous ceramic structures[27] show very interesting properties,[28-30] and may be combined with macroscopically designed paper-templated ceramics.[31] By combining

specific functional groups within mesopores, transport can be gated in response to external stimuli such as temperature[32], pH[33-35], specific molecules[36-37], voltage,[38-40] and light.[41-43] Here, we use sol-gel chemistry to design functional mesopores within cotton-linter paper. We investigate the effect of the presence and absence of these mesopores, the paper grammage, and hydrophobization on the fluid flow. Using redox-responsive polymers, we can dynamically switch from water exclusion to capillary fluid flow.

EXPERIMENTAL DETAILS

Reagents. All chemicals and solvents were purchased from Fisher Scientific, Merck, Sigma-Aldrich or Alfa Aesar, and used as received unless otherwise stated. Cu(I)Cl was washed five times with glacial acetic acid and ethanol. *N*-,*N*-,*N'*-,*N'*-,*N''*-Pentamethyldiethylenetriamine (PMDETA), anisole, *2*-bromo-*iso*-butyric *tert*-butylester (*t*BbiB) were degassed and stored under an inert argon atmosphere or in a glovebox. Toluene was distilled from sodium/benzophenone. The copper complexes were freshly prepared in anisole and treated in the glovebox. The ATRP initiator, 3-(2-bromoisobutyrate)propyl trichlorosilane,[44] as well as the 2-(methacryloyloxy)ethyl ferrocenecarboxylate monomer (FcMA)[45] were both synthesized in accordance to literature procedures described elsewhere.

Paper fabrication. For the preparation of the Cotton Linter paper substrates, bleached, dry Cotton Linter pulp was used. The pulp was refined in a Voith LR 40 laboratory refiner. Refining was performed with an effective specific energy of 200 kWh t^{-1}. Cotton Linter paper sheets with a grammage of 42-44 g m^{-2} were fabricated using a conventional Rapid-Koethen hand sheet maker according to DIN 54358 and ISO 5269/2 in the absence of additives and fillers. After sheet formation, the paper substrates were equilibrated at a temperature of 23 °C and a relative humidity of 50 % in a climate-controlled room for at least 24 h before further characterization

was performed. After which time, the paper sheets on average contained approximately 6 % water due to adsorption from the humid air.

Mesoporous and dense silica coatings were synthesized via sol−gel chemistry based on the oxide precursor tetraethoxysilane (TEOS) in the presence of a Pluronic® F127 template. Dynamic light scattering (DLS) measurements under the conditions used in the coating procedure of this study (acidic ethanol) reveal a concentration-independent micelle diameter of 6.8 ± 0.5 nm for Pluronic® F127 concentrations between 0.3 and 9.3 mg/mL. This indicates the Pluronic® F127 forms spherical micelles under the coating conditions used. To prepare mesoporous silica coatings, the precursor solution was prepared using the following molar ratios: 1 TEOS : 0.075 (or 0.005, Figure S1) Pluronic® F127 : 24 EtOH : 5.2 H_2O : 0.28 HCl. Dense silica coatings were prepared similarly, but it the absence of the Pluronic® F127 template. The precursor solution was stirred for 24 h and used to produce films via evaporation-induced self-assembly (EISA)[27] on Cotton Linter paper sheets at 40−50 % relative humidity and 298 K at a withdrawal speed of 2 mm s^{-1}. Freshly deposited films were stored at 50 % relative humidity in a climate chamber for 1 h. A consecutive thermal treatment was then carried out in two successive 1 h steps at 60 and 130 °C, followed by a temperature increase to either 200 or 500 °C, respectively, at a rate of 1 °C min^{-1}. This final temperature was held for 2 h before cooling to ambient temperature. The prepared samples were then rinsed with ethanol and stored under ambient conditions. The samples that were treated up to a temperature of 200 °C were then immersed into acidic ethanol (0.01 M HCl) to chemically extract the Pluronic® F127 template. To prepare Cotton Linter paper sheets that were coated only within one half with dense silica, the samples were stored in a preheated oven at 130 °C for 1 h immediately after dip-coating, followed by a temperature increase to 200 °C at a rate of 1 °C min^{-1}.

Immobilization of the ATRP Initiator. The ceramic papers were placed into a Schlenk tube before being dried under vacuum. Under an inert argon atmosphere, dry toluene (20 mL) and

3-(2-bromoisobutyrate)propyl trichlorosilane (1 g, 2.92 mmol) were added. After stirring at 60 °C for 24 h, the papers were rinsed with THF, MeOH, and water, followed by drying under reduced pressure.

Surface-Initiated ATRP of FcMA. The initiator-functionalized papers were placed in a Schlenk tube, and then dried under vacuum before being backfilled with argon. Anisole (dense 1: 15 mL – dense 2/F127: 18 mL), FcMA (960 mg; 2.810 mmol), and 2-bromo-*iso*-butyric *tert*-butylester (*t*BbiB) (10 µL, 0.054 mmol) were then added. The reaction mixture was then heated to a temperature of 90 °C before the polymerization was initiated by adding a solution of [Cu^{I}(PMDETA)Cl] (0.2 M, 1 mL, 0.2 mmol in anisole). After 24 h, the polymerization was quenched by pouring the solution into MeOH, and the paper was rinsed successively with THF, MeOH, water, and finally THF before drying *in vacuo*. The precipitated polymer was collected by filtration, dried under reduced pressure, and characterized by size exclusion chromatography (SEC). The corresponding SEC data is detailed in Table 1.

Table 1: Molar masses, dispersity, and degree of polymerization of the free PFcMA formed in solution as reference.

Sample	M_n / g mol^{-1} [a]	M_w / g mol^{-1} [a]	$Đ_M$[a]	*PDI*
PFcMA$_{12}$ dense 1	4000	5600	1.41	12
PFcMA$_{20}$ dense 2	6900	10500	1.52	20
PFcMA$_{20}$ F127				

[a] determined by SEC equipped with a UV detector against PS standards.

Oxidation of the ferrocene-containing polymers. The papers were placed in DCM (15 mL) and treated with 50 mg (0.06 mmol) tris(4-bromophenyl) ammoniumyl hexachloroantimonate, or in THF (15 mL) with 50 mg (0.31 mmol) of $FeCl_3$ for 16 h, respectively. The papers were repeatedly rinsed with THF and water before drying under ambient conditions overnight.

Electron microscopy. Scanning electron microscopy **(**SEM) micrographs were captured using a JEOL JSM-6510 scanning microscope operated at an acceleration voltage of 20 kV. Samples were coated with a platinum/palladium layer of several nanometers. Transmission electron microscopy (TEM) micrographs were recorded using a FEI CM20 TEM microscope with a maximum resolution of 2.3 Å equipped with a LAB-6 cathode and a CCD camera (Olympus). Samples were dispersed in a few droplets of ethanol before being dropped onto a copper TEM grid to image.

Contact angle. Contact angle measurements were carried out using Modell TBU90E Dataphysics instruments GmBH with the Programm SCA-Software. All samples were measured at five positions, and the average value calculated with standard deviation. For static contact angle measurements, a water drop volume of 3 μL was used.

Water penetration. Capillary-driven water penetration was performed in a 100 mL beaker filled with 8 mL of distilled water. The samples were immersed into the water reservoir up to 3 mm, while ensuring a perpendicular orientation to the water surface. The capillary-driven water flow was then recorded with a camera.

Infrared (IR) spectroscopy was performed on a Spectrum One instrument (Perkin−Elmer) in attenuated total reflection (ATR) mode. IR spectra were recorded from 4000 to 600 cm^{-1}. The measured spectra were automatically background-corrected and normalized to the Si−O−Si band at ∼1070 cm^{-1}.

Solid-State NMR spectroscopy. ^{29}Si CP MAS spectra were recorded on a Bruker Avance III HD 600 spectrometer at room temperature employing a 4 mm broad band H/X probe. Spectra were measured at 14 T, corresponding to a frequency of 119.22 MHz for ^{29}Si, and at 8 kHz spinning. All spectra were referenced to TMS, and kaolin was employed as an external standard (-92.5 ppm). The ramped CP-MAS sequence[46] was utilized with a contact time of 2 ms and a

recycle delay of 1-2 s. Spectra were accumulated from 64k scans. Tppm decoupling,[47] employing a 15° phase jump, was applied during data acquisition.

Fluorescence microscopy. Confocal recordings were performed as described earlier.[11] An aqueous FITC-Dextran solution (0.1 mg mL^{-1}) was supplied at the uncoated half of a silica-coated paper strip, placed on a hydrophobic coverslip (HybriSlip™, 24 x 60mm, Sigma-Aldrich Chemie GmbH, Munich, Germany), and imaged on a Leica SP5II confocal microscope (Leica Microsystems GmbH, Mannheim, Germany) using a 10x objective. Images were recorded by sequentially exciting each pixel line of the scan with 405 and 488 nm, and the autofluorescence emission of the cellulose fibers between 420 and 460 nm collected in addition to the emission of FITC between 500 and 550 nm. As FITC is also excited at 405 nm, a mild bleed through of the FITC-signal is visible in the channel to detect the autofluorescence emission of the cellulose fibers (Figure 5, b).

RESULTS AND DISCUSSION

To investigate the influence of structurally defined and functionalized porous coatings on the capillary fluid transport of Cotton Linter paper sheets, sol-gel chemistry and post-grafting strategies were applied. The coatings applied onto the constituent cellulosic fibers of the paper sheets with mesoporous or dense silica, and its subsequent functionalization, is schematically depicted in Figure 1. Depending on the presence or absence of the micelle forming block copolymer template (Pluronic® F127), a mesoporous or dense silica coating was obtained on the cellulose paper fibers. In addition, temperature treatments can also be adjusted to further obtain either mesoporous silica-paper hybrid materials (heating up to 200 °C) or pure silica paper-derived materials (heating up to 500 °C). Note, the latter refers to purely ceramic materials where the organic fibers are being burned to yield a silica-based structure. Further functionalization of both pure ceramic and paper-silica hybrid materials is either carried out by gas phase deposition of hydrophobic silanes such as 1H,2H,2H,2H-

perfluorooctyltrichlorosilane (PFOTS) and 1H,1H,2H,2H-perfluoroctyldimethylcholorsilane (PFOMS) (see Supporting Information for details), or by surface-initiated atom transfer radical polymerization (SI-ATRP) to yield a redox-responsive polymer-coating at the silica surface of poly(2-(methacryloyloxy)ethyl ferrocenecarboxylate) (PFcMA). To generate such redox-responsive coatings, initiators capable of undergoing ATRP were first immobilized onto the silica-coated paper, allowing the subsequent polymerization of redox-responsive 2-(methacryloyloxy)ethyl ferrocenecarboxylate (FcMA). Such polymer coatings can be used to reversibly switch the surface polarity upon oxidation/reduction cycles.[26] It must be noted that if cellulose surface hydroxyl groups are still present and accessible after performing the silica modification, initiator binding to these hydroxyl groups[48] cannot be excluded.

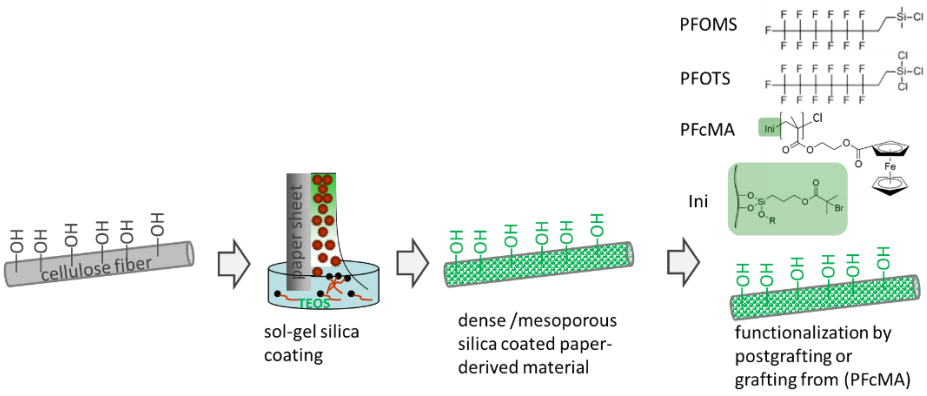

Figure 1: Schematic illustration of the preparation process used to generate paper-derived mesoporous silica sheets and their functionalization using either hydrophobic silanes (PFOMS or PFOTS) in a grafting-to approach, or by the preparation of a redox-responsive polymer-coating by a grafting-from approach.

After the silica-paper hybrid materials were prepared, the resulting morphology was investigated by electron microscopy. Figure 2 a,b demonstrates that an intact fibrous structure of mesoporous silica-coated Cotton Linter paper (44 g m^{-2}) resulted after treatment at 200 °C. The electron micrograph of the sample treated up to 500 °C shows the typical fiber morphology has been disrupted (Figure 2 c,d). Investigating the surface morphology of the fibers shown in Figure 2 c,d via TEM further reveals a mesoporous structure with the formation of ordered

pores smaller than 10 nm in the presence of the Pluronic® F127 template during silica formation (Figure 2 e,f). When comparing the mesoporous paper-derived silica structure after burning off the cellulose fibers (Figure 2 c,d) with the paper-derived dense silica structure (no mesopore template present in the sol-gel coating process) after burning off the cellulose fibers (Figure 2 g,h) the fiber structure is notably disrupted in both materials.

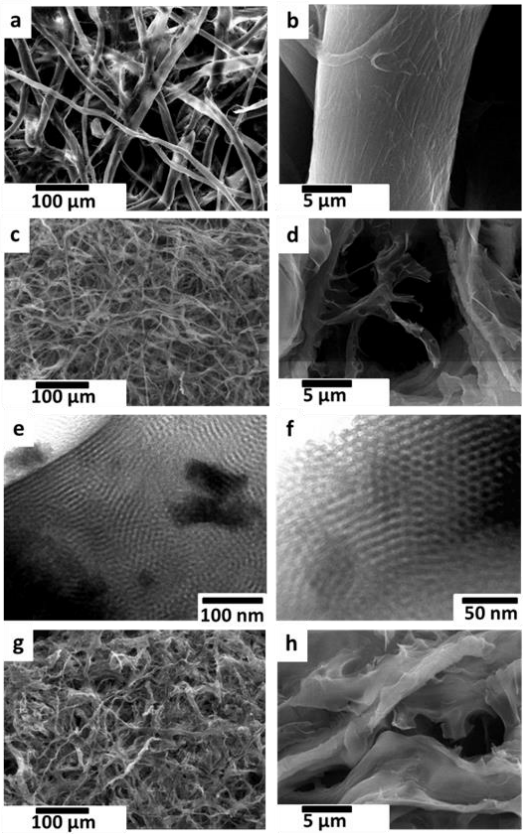

Figure 2: Electron microscopy images of Cotton Linter (44 g m^{-2}) paper-derived silica structures: a, b) SEM images of mesoporous (F127) paper-derived silica treated to 200 °C without destroying the cellulosic paper structure; c,d) SEM images of mesoporous (F127) paper-derived silica treated to 500 °C; e,f) TEM images resolving the mesoporous structure of mesoporous (F127) paper-derived silica treated to 500 °C, and g,h) non-mesoporous paper-derived silica treated until 500 °C.

The presence or absence of cellulosic fibers, as well as further functionalization of the fiber surface, was confirmed by infrared spectroscopy (Figure 3). Infrared spectra of bare Cotton Linter paper, mesoporous or dense silica-coated hybrid paper (treated up to 200 °C), and paper-derived silica paper (treated up to 500 °C), as well as the IR spectra after functionalization with a redox responsive polymer, PFcMA, show characteristic vibrational bands at 1728 and 1070

cm^{-1}, which correspond to the C=O vibration of PFcMA and Si−O−Si stretching, respectively. These observations confirm the presence of the mesoporous or dense silica, and their successful modification.[49] Whilst the cellulose fibers exhibit a complex infrared spectrum (Figure 3a, black) that overlaps with the silica vibrational bands at 1070 cm^{-1} (Figure 3a, red), the silica structure is clearly observable after removing the cellulose fibers by heating at 500 °C for 2 h (Figure 3a, green). After the removal of the cellulosic material, the resulting brittle ceramic material (Figure S3) exhibits an infrared spectrum similar to pure silica films (Figure 3b). Functionalization with PFOMS or PFOTS does not result in any significant changes to the infrared spectrum. The C-F stretching vibration between 1400 and 1000 cm^{-1} is hidden beneath the cellulose and silica vibrational bands. Nevertheless, this observation indicates the stability of cellulose and silica after PFOMS and PFOTS functionalization, and is in accordance with TEM and ellipsometry results (Figure S1). The PFcMA functionalization becomes evident by a small absorption band at 1728 cm^{-1} corresponding to the C=O vibration of the PFcMA. The comparably small absorption is due to the low amount of polymer present relative to cellulose in the mesoporous silica-coated hybrid paper. Nevertheless, functionalization with PFcMA can clearly be proven for paper-derived silica (without cellulose fibers), and subsequent polymer functionalization (Figure 3b). Additionally, no difference in the C=O vibrational band at 1728 cm^{-1} relative to the Si-O-Si matrix at 1070 cm^{-1} can be observed before and after the oxidation of PFcMA with $FeCl_3$. This clearly indicates that differences in the interaction with water upon oxidation and reduction are due to the different surface energies and not due to material instability, i.e., changes in the morphology of the paper sheet.

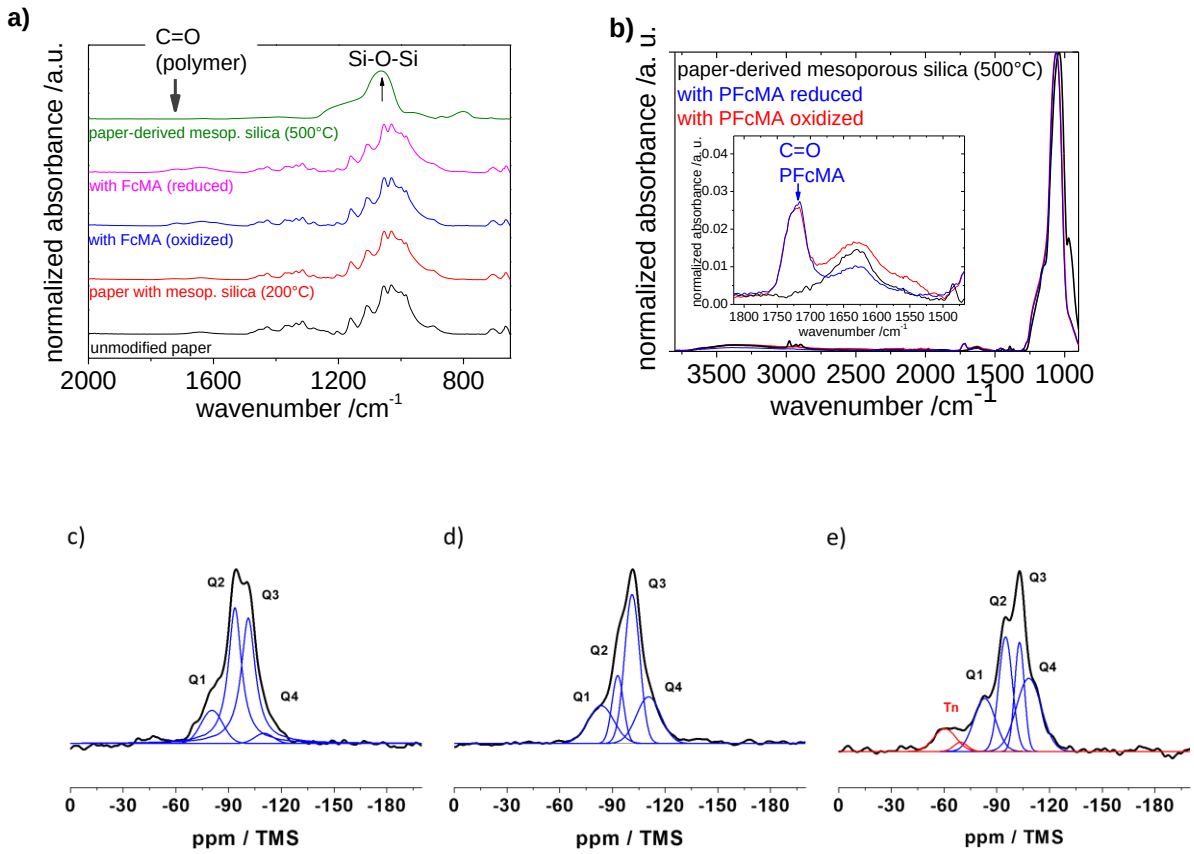

Figure 3: a) Infrared spectra of untreated paper sheets (Cotton Linters, 44 g m^{-2}, black), mesoporous silica hybrid paper sheets (200 °C) (red), mesoporous silica hybrid paper sheets (200 °C) functionalized with PFcMA in an oxidized (blue) and reduced (pink) state, and paper-derived mesoporous silica after destroying the cellulose paper fibers at 500 °C (green); b) infrared spectra of untreated paper–derived mesoporous silica after destroying the cellulose fibers at 500 °C unmodified (black), and functionalized with PFcMA in a reduced (blue) and oxidized (red) state; c) ^{29}Si-CP-MAS NMR spectra measured at 8 kHz spinning of paper hybrid mesoporous silica (200 °C), and d) of paper-derived mesoporous silica (500 °C); e) ^{29}Si-CP-MAS NMR spectra measured at 8 kHz spinning of PFcMA-functionalized paper hybrid mesoporous silica (200 °C).

The successful silica functionalization was additionally confirmed by ^{29}Si CP-MAS NMR spectroscopy measured before and after PFcMA grafting. The spectra shown in Figure 3c, d illustrate the typical pattern for non-functionalized porous silica represented by Q_n groups between approximately -80 and -115 ppm. After functionalization of the mesoporous hybrid paper-based silica with PFcMA (Figure 3e) T_n groups in the range of -60 to -70 ppm appear. This result indicates a covalent binding of functional groups (PFcMA polymer, or ATRP initiator) to the silica via the silane anchoring groups. Additionally, the relative intensities of

the Q_n signals between -80 and -115 ppm change after the functionalization with PFcMA (Figure 3e). Although the ^{29}Si-CP-MAS NRM spectra cannot be evaluated quantitatively, a decrease of the relative amount of the OH bearing groups (Q_1, Q_2 and Q_3) is observed compared to Q_4. This further indicates the successful reaction of silica hydroxyl groups with the silane anchoring groups. Interestingly, the Q_1 groups at approximately -81 ppm are detected in all spectra. In most studies, the Q_1 groups are not observed for pure mesoporous silica materials such as SBA-3 or MCM-41,[50] as well as for the cellulose/silica hybrid materials[51-53] or cellulose derivatives immobilized on silica.[54-55] The presence of such Q_1 groups depends on the aging time in the applied sol-gel process[56] and seems to be additionally influenced by the presence of cellulose paper fibers. After heating the mesoporous silica-coated sample to 500 °C, the cellulose matrix decomposed as illustrated in the ^{13}C-CP-MAS spectrum (Supporting Information, Figure S3c). The characteristic signals of cellulose between 60 and 120 ppm are no longer observed. Only very broad signals, likely originating from the carbonized paper, are visible after accumulating a large number of scans.

The change in the relative intensities of the different Q groups in the ^{29}Si-CP-MAS spectra for paper-based hybrid mesoporous silica (200 °C) and paper-derived mesoporous silica (500 °C) (Figure 3c and 3d) indicate that the cross-linking process is stimulated by heating. Nevertheless, the structural framework of the silica, which is given by the organization of the paper template, appears to be mostly preserved during the calcination since the Q_1 signals are still observed.

Dense versus mesoporous silica coatings: capillary-driven fluid flow

The interactions, and hence, the possibility of fluid transport modulation of water by capillary forces within the different materials and hybrid materials prepared was investigated. A significantly higher static contact angle is observed for unmodified dense silica-paper hybrid materials in comparison to mesoporous silica-paper hybrid materials. The corresponding capillary-rise tests show no water fluid flow in dense silica-paper hybrid materials as shown in

Figure 4. On coating a paper sheet partially with dense silica (Figure 4a), a fluid stop barrier is created that is even visible by eye (Figure 4a,b,f). Note, this effect is observed without the addition of any functional component to the silica coating. Even though the water contact angle on dense silica is considerably small, water does not rise as a consequence of small capillary forces presumably. In order to prove this hypothesis we varied the paper porosity by preparing paper sheets from Cotton Linter fibers having different grammages .[4] Up to a critical grammage with dense silica coatings on cellulose fibers, no water imbibition is observed (Figure S2). The exact value of this critical grammage strongly depends on the exact paper fiber morphology and hierarchical sheet porosity. These observations indicate that water penetration is not only affected by the inter-fiber porosity, which is often used to explain Lucas-Washburn-like capillary fluid flow, but is also strongly affected by fiber morphology.

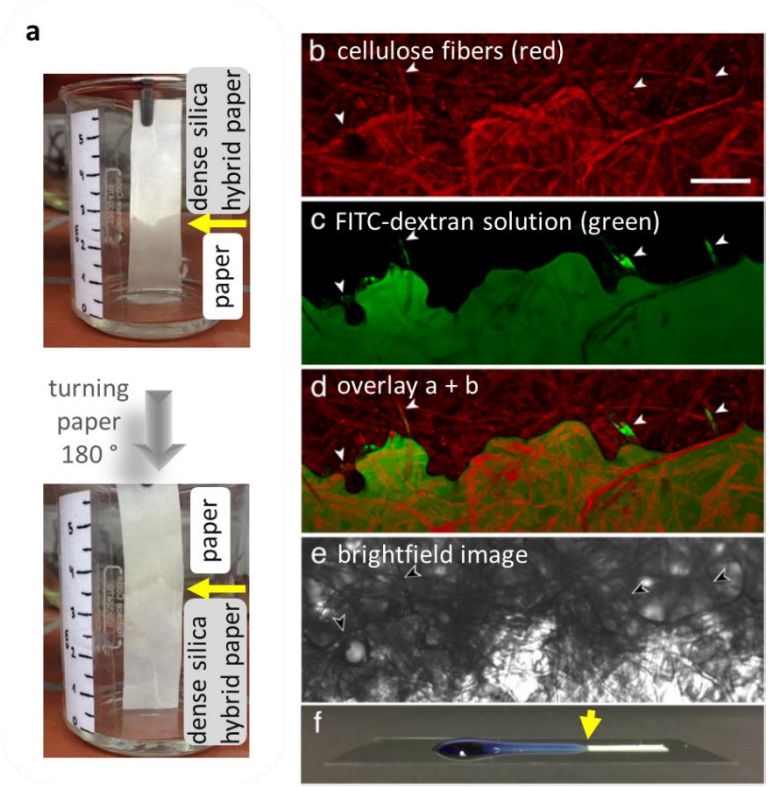

Figure 4: a) Water capillary uptake of Cotton Linter paper sheets coated in one half with dense silica. b-e) maximum projections of a stack of confocal images taken at the border between the uncoated and silica-coated area of a paper strip (bottom and top half of images a-d, respectively). Autofluorescence of cellulose fibers (b), FITC-Dextran solution (c), overlay (d), and brightfield image (e). Scale bar = 200 µm. f) Photograph of the stopping dye-containing water fluid front. For comparison the water front passing the border between a mesoporous

silica coating and unmodified Cotton Linter paper is shown in the supporting information (Figure S7).

In order to understand this in more detail, fluorescence microscopy analysis on water imbibition was carried out where the aqueous phase carries a dissolved FITC-Dextran, causing a green fluorescence, and the dense silica-coated cellulose fibers a red autofluorescence (Figure 4b-f). The solution, including the dye, is taken up by the uncoated half of the paper strip (Figure 4c). No propagation into the dense silica-coated area is observed even though the fibers clearly continue, and the inter-fiber space does not change at the observed scales. Only a few streaks of liquid show capillary transport of the FITC-Dextran solution on the surface, and this likely results from cellulose fibers that are not completely coated within this border region (arrowheads). The obtained fluorescence microscopy images suggest the capillary uptake of FITC-labeled dextran containing water within the unmodified Cotton Linter paper sheet and that capillary-driven fluid flow comes to a stop at the border with the dense silica-coated region of the paper sheet. The fiber morphology (red fluorescence) is clearly visible, and no significant differences are observed between the unmodified and dense silica-coated fibers and a stopping fluid front containing green fluorescent FITC labelled dextran. The influence of a dense versus mesoporous silica coating at which this fluid exclusion behavior is not observed gives interesting insight into the transport mechanisms in paper, which seem to be strongly related to the fiber (porous) morphology and fiber surface.

Gradual tuning and redox-gating of capillary-driven fluid flow

A gradual tuning of the wetting properties by adjusting the hydrophobicity and thus water flow was achieved by grafting the hydrophobic silanes PFOTS or PFOMS to the mesoporous silica hybrid paper matrix with varying functionalization time. Planar mesoporous silica films are used as reference (Figure S1). These experiments show water penetration for contact angles below approximately 100 °, with gradual tuning of the wetting and water penetration, as well

as water exclusion from the porous silica fiber morphology after surface modification resulting in contact angles higher than 100 °. The results obtained from the hydrophobization using silanization confirm that gating water flow in such silica-based fiber morphologies occurs when contact angles are switched from above 100 ° to well below 100 °. To achieve this gating by external stimuli, mesoporous silica-paper hybrid sheets (Figure 2a,b) were functionalized with PFcMA in a grafting-from approach using ATRP after functionalizing the dense or mesoporous silica-paper hybrid sheets (44 g m^{-2}) with the ATRP initiator.[21, 26] The presence of polymer before and after oxidation is confirmed by infrared spectroscopy (Figure 3). For the silica hybrid paper (200 °C) after functionalization with PFcMA in the reduced state, contact angles of 105-120 ° (Figure 5) are observed, which correspond to water exclusion from the fibrous matrix. After oxidation of the PFcMA, the measured contact angle drops to 60-80 ° (Figure 5), switching from a hydrophobic to a hydrophilic state, and consequently from water exclusion to capillary water flow into the mesoporous silica hybrid paper sheet. This works for mesoporous and dense silica coatings in which at least a slight water penetration is observed before polymer functionalization. For dense silica coatings this observation is surprising and reference experiments show fast water penetration after incubation of dense silica-coated paper samples in THF. This also indicates the role of the fiber itself. THF leads to swelling of the cellulose fibers, which likely results in the rupture of the dense silica coating. The water can then access the cellulose fiber. Incubation of dense hybrid silica paper in toluene does not result in the same switching behavior from hydrophobic to hydrophilic, and the dense hybrid silica paper excludes water even after toluene incubation. Toluene is reported to show a low cellulose fiber swelling potential.[57] Nevertheless, in all cases this oxidation-based change of fluid flow is reversible and a repeated reduction leads again to contact angles above 100 °, even if the absolute values are slightly lower than before oxidation (Figure S5). This clearly demonstrates the effect of the redox polymer. The paper-derived silica sheets (500 °C, after burning off the cellulose fibers) are relatively brittle and not ideally flat which makes them difficult to handle in synthesis and

characterization experiments. Nevertheless, the contact angle behavior for unmodified and PFcMA-modified paper-derived silica sheets were comparable, showing immediate water uptake before PFcMA functionalization. Contact angles greater than 100 °, and up to 120 ° in the case of functionalization with reduced PFcMA were observed, and could be decreased to 40-80 ° upon oxidation with iron(III)chloride in THF to permit water penetration.

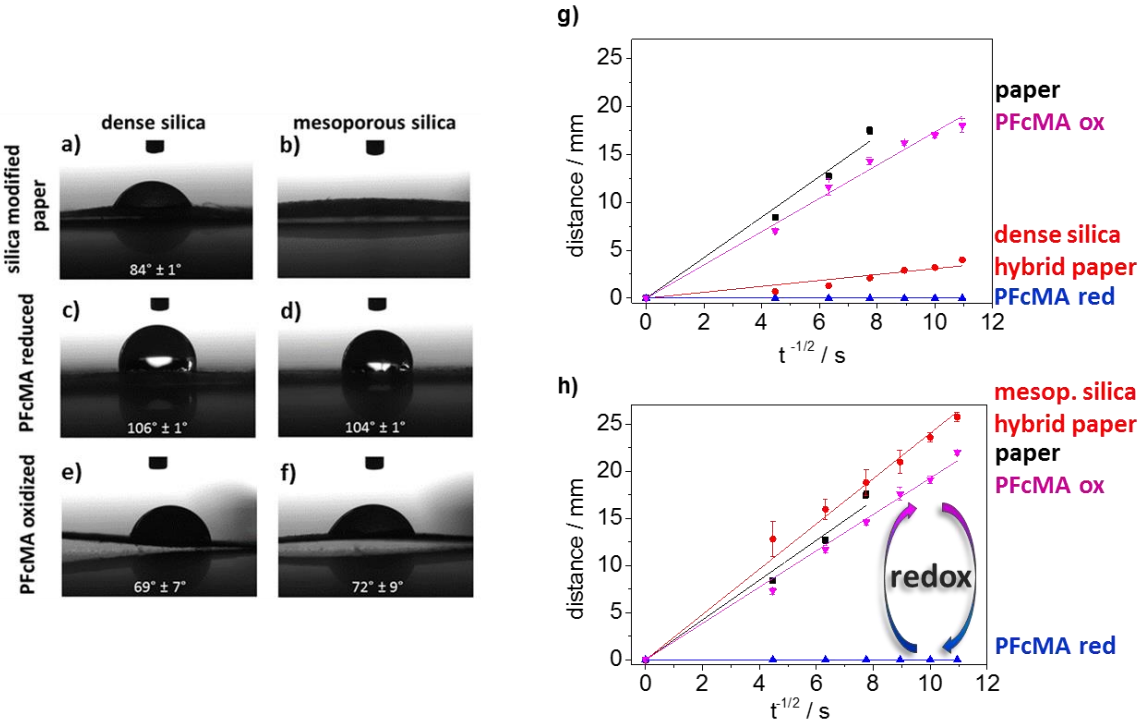

Figure 5: Contact angle of silica-modified hybrid paper before (a, b) and after (c-f) PFcMA modification: a) dense silica hybrid paper; b) mesoporous silica hybrid paper. The influence of reduced PFcMA in dense (c) and mesoporous (d) silica hybrid paper versus chemically oxidized PFcMA in dense (e) and mesoporous (f) silica hybrid paper is clearly visible and follows a Cassie-Wenzel-like transition. g, h) Capillary water fluid flow measured for g) Cotton Linter paper (44 g m^{-2}) (black), dense silica hybrid paper (200 °C, red), dense silica hybrid paper after PFcMA modification in the reduced (blue) state and after oxidation with $FeCl_3$ (pink). h) Capillary water fluid flow measured for Cotton Linter paper (44 g m^{-2}) (black), mesoporous silica hybrid paper (200 °C, red), mesoporous silica hybrid paper after PFcMA modification in the reduced (blue) state, and after oxidation with $FeCl_3$ (pink).

Capillary water uptake is fast for unmodified paper and for mesoporous silica-paper hybrid materials, and are comparable to pure Cotton Linter paper (~ 44 g m^{-2}) (Figure 5h black, red). The mesoporous silica-paper hybrid material requires approximately 120 s for water penetration up to a distance of 2.6 cm, within the experimental error, similarly to unmodified

Cotton Linter paper. A linear dependence of the capillary rise on the square root of time, according to Lucas-Washburn equation, results in slopes of 2.1 for the unmodified Cotton Linter paper and 2.3 for the unfunctionalized mesoporous silica-paper hybrid sheet. Both materials are hydrophilic and exhibit a slow water imbibition if a drop of water is placed on top of the material, i.e., during contact angle measurements. Hence, the mesoporous silica coating does not appear to affect the water penetration significantly. Interestingly, the water penetration is significantly slower when a dense silica coating is applied in comparison to a mesoporous silica coating (Figure 5g), as previously discussed. At 120 seconds, i.e., $t^{1/2}$ is approximately 11, water penetrates these hybrid materials only ~3 mm (red circles in Figure 5), which corresponds to a slope according to Lucas-Washburn of approximately 0.3. This observation is in line with the higher contact angles measured for these materials and supports the hypothesis of the fiber interface or interior space playing a major role in water imbibition of paper-based or paper-like materials. The functionalization of these silica-paper hybrid materials with redox-responsive PFcMA in its reduced state results in complete water exclusion (Figure 5, blue triangles) for at least 8 h. Gating to water penetration is achieved upon oxidation of the PFcMA if a sufficient amount of ferrocene units are oxidized. Water penetration for 120 s travels a distance of 2.2 cm after PFcMA oxidation in the mesoporous silica-paper hybrid material (Figure 5h, pink), and 1.8 cm in the dense silica-paper hybrid material (Figure 5g, pink). A linear fitting according to the Lucas-Washburn equation results in a slope of 1.9 and 1.7 for the mesoporous silica-paper hybrid material and the dense silica-paper hybrid material, respectively. Furthermore, the slope of 1.9 for the PFcMA-functionalized mesoporous silica-paper hybrid material is similar to the polymer-free mesoporous silica-paper hybrid material of 2.1, which shows real gating of water penetration. Although the exact fluid flow depends on the exact hierarchical paper sheet morphology (Figure S2), these results clearly show that redox-gating of water penetration into paper-derived materials is possible if a contact angle

change close to the transition from a Cassie-type wetting (no water imbibition) to a Wenzel-type wetting (water imbibition) is achieved.

CONCLUSIONS

Based on sol-gel silica coatings, capillary water fluid flow in silica hybrid paper sheets can be gradually adjusted. A dense silica coating on Cotton Linter cellulose fibers is able to completely block the capillary driven water imbibition into silica hybrid paper sheets without any further chemical hydrophobization of the fiber surfaces. Incubation of dense silica hybrid paper sheets in THF leads to fast water penetration, which further indicates the role of the fiber itself and the cellulose fiber swelling in capillary fluid flow. In contrast to dense silica coatings, mesoporous silica coatings on Cotton Linter cellulose fibers show capillary water transport comparable to unmodified paper sheets. Incubation in THF, modification of silica-coated paper hybrid materials (dense or mesoporous), as well as paper-derived pure silica materials with redox-responsive PFcMA polymers, allows us to dynamically and reversibly switch from water exclusion to water imbibition upon oxidation. This study reports the first successful steps towards programmable fluid flow and molecular passage control in hierarchically porous paper-based materials, where capillary driven fluid transport can be gated by an external redox-switch. The latter, in particular, offers large potential for dynamic fluid and molecular transport control in paper-derived low-cost lab-on-chip devices. Finally, the presented results indicate that independently designing fiber morphology (roughness) and functionalization would be a key step towards rationally defined wetting properties.

ASSOCIATED CONTENT

Supporting Information available.

AUTHOR INFORMATION

Corresponding Author

*brunsen @cellulose.tu-darmstadt.de

Author Contributions
All authors have given approval to the final version of the manuscript.

ACKNOWLEDGMENT
The authors would like to thank the Fonds der Chemischen Industrie and the LOEWE project iNAPO by the Hessen State Ministry of Higher Education, Research and the Arts for financial support of this work. Christelle Dubois gratefully acknowledges the Erasmus Program for funding. Stefanie Richter and Tizian Venter are gratefully acknowledged for preparation of the unmodified paper substrates, Laura Silies for support with SEM measurements, and Gerd Buntkowsky for measurement time at his 600 MHz Bruker Avance III HD spectrometer to perform the solid-state NMR experiments. Jessica Tom is gratefully acknowledged for language editing.

References

1. Geldner, N., The endodermis, *Annu. Rev. Plant Biol.* **2013,** *64*, 531-558.
2. Martinez, A. W.; Phillips, S. T.; Whitesides, G. M., Three-dimensional microfluidic devices fabricated in layered paper and tape, *Proc. Natl. Acad. Sci. U.S.A.* **2008,** *105*, 19606-19611.
3. Martinez, A. W.; Phillips, S. T.; Butte, M. J.; Whitesides, G. M., Patterned paper as a platform for inexpensive, low-volume, portable bioassays, *Angew. Chem. Int. Ed.* **2007,** *46*, 1318-1320.
4. Böhm, A.; Carstens, F.; Trieb, C.; Schabel, S.; Biesalski, M., Engineering microfluidic papers: effect of fiber source and paper sheet properties on capillary-driven fluid flow, *Microfluid. Nanofluid.* **2014,** *16*, 789-799.
5. Noh, H.; Phillips, S. T., Metering the Capillary-Driven Flow of Fluids in Paper-Based Microfluidic Devices, *Anal. Chem.* **2010,** *82*, 4181-4187.
6. Cheng, C. M.; Martinez, A. W.; Gong, J.; Mace, C. R.; Phillips, S. T.; Carrilho, E.; Mirica, K. A.; Whitesides, G. M., Paper-based ELISA, *Angew. Chem. Int. Ed.* **2010,** *49*, 4771-4774.
7. Songjaroen, T.; Dungchai, W.; Chailapakul, O.; Henry, C. S.; Laiwattanapaisal, W., Blood separation on microfluidic paper-based analytical devices, *Lab Chip* **2012,** *12*, 3392-3398.
8. Martinez, A. W.; Phillips, S. T.; Whitesides, G. M., Diagnostics for the Developing World: Microfluidic Paper-Based Analytical Devices, *Anal. Chem.* **2010**, 3-10.
9. Li, X.; Ballerini, D. R.; Shen, W., A perspective on paper-based microfluidics: Current status and future trends, *Biomicrofluidics* **2012,** *6*, 011301-13.
10. Lisowski, P.; Zarzycki, P. K., Microfluidic Paper-Based Analytical Devices (lPADs) and Micro Total Analysis Systems (lTAS): Development, Applications and Future Trends, *Chromatographia* **2013,** *76*, 1201-1214.
11. Bump, S.; Boehm, A.; Babel, L.; Wendenburg, S.; Castens, F.; Schabel, S.; M., B.; Meckel, T., Spatial, spectral, radiometric and temporal analysis of polymer-modified paper substrates using fluorescence microscopy, *Cellulose* **2015,** *22*, 73-88.

12. Böhm, A.; Gattermayer, M.; Trieb, C.; Schabel, S.; Fiedler, D.; Miletzky, F.; Biesalski, M., Photo-attching functional polymers to cellulose fibers for the design of chemically modified paper, *Cellulose* **2013,** *20*, 467-483.
13. Carrilho, E.; Martinez, A. W.; Whitesides, G. M., Understanding Wax Printing: A Simple Micropatterning Process for Paper-Based Microfluidics, *Anal. Chem.* **2009,** *81*, 7091-7095.
14. Giokas, D. L.; Tsogas, G. Z.; Vlessidis, A. G., Programming Fluid Transport in Paper-Based Microfluidic Devices Using Razor-Crafted Open Channels *Anal. Chem.* **2014,** *86*, 6202-6207.
15. Yamada, K.; Henares, T. G.; Suzuku, K.; Cittero, D., Papierbasierte tintenstrahlgedruckte Mikrofluidiksysteme für die Analytik, *Angew. Chem.* **2015,** *127*, 5384-5401.
16. Janko, M.; Jocher, M.; Boehm, A.; Babel, L.; Bump, S.; Biesalski, M.; Meckel, T.; Stark, R. W., Cross-Linking Cellulosic Fibers with Photoreactive Polymers: Visualization with Confocal Raman and Fluorescence Microscopy, *Biomacromol.* **2015,** *16*, 2179-2187.
17. Sun, W.; Zhou, S.; You, B.; Wu, L., A facile method for the fabrication of superhydrophobic films with multiresponsive and reversibly tunable wettability, *J. Mater. Chem. A* **2013,** *1*, 3146-3154.
18. Shi, F.; Song, Y.; Niu, J.; Xia, X.; Wang, Z.; Zhang, X., Facile Method To Fabricate a Large-Scale Superhydrophobic Surface by Galvanic Cell Reaction, *Chem. Mater.* **2006,** *18*, 1365-1368.
19. C. L. Feng; Zhang, Y. J.; Jin, J.; Song, Y. L.; Xie, L. Y.; Qu, G. R.; Jiang, L.; Zhu, D. B., Reversible Wettability of Photoresponsive Fluorine-Containing Azobenzene Polymer in Langmuir-Blodgett Films, *Langmuir* **2001,** *17*, 4593-4597.
20. Pei, Y.; Travas-Sejdic, J.; Williams, D. E., Reversible electrochemical switching of polymer brushes grafted onto conducting polymer films, *Langmuir* **2012,** *28*, 8072-8083.
21. Elbert, J.; Krohm, F.; Rüttiger, C.; Kienle, S.; Didzoleit, H.; Balzer, B. N.; Hugel, T.; Stühn, B.; Gallei, M.; Brunsen, A., Polymer-Modifi ed Mesoporous Silica Thin Films for Redox-Mediated Selective Membrane Gating, *Adv. Funct. Mater.* **2014,** *24*, 1591-1601.
22. Xin, B.; Hao, J., Reversibly switchable wettability, *Chemical Society reviews* **2010,** *39*, 769-782.
23. Drelich, J.; Chibowski, E.; Meng, D. D.; Terpilowski, K., Hydrophilic and superhydrophilic surfaces and materials, *Soft Matter* **2011,** *7*, 9804-9828.
24. Alexander, S.; Eastoe, J.; Lord, A. M.; Guittard, F.; Barron, A. R., Branched Hydrocarbon Low Surface Energy Materials for Superhydrophobic Nanoparticle Derived Surfaces, *ACS Appl. Mater. Interf.* **2016,** *8*, 660-666.
25. Rüttiger, C.; Mehlhase, S.; Vowinkel, S.; Cherkashinin, G.; Liu, N.; Dietz, C.; Stark, R. W.; Biesalski, M.; Gallei, M., Redox-mediated flux control in functional paper, *Polymer* **2016,** *DOI 10.1016/j.polymer.2016.01.065*.
26. Elbert, J.; Gallei, M.; Rüttiger, C.; Brunsen, A.; Didzoleit, H.; Stühn, B.; Rehahn, M., Ferrocene Polymers for Switchable Surface Wettability, *Organometallics* **2013,** *32*, 5873-5878.
27. Brinker, C. J.; Lu, Y.; Sellinger, A.; Fan, H., Evaporation-Induced Self-Assembly: Nanostructures Made Easy, *Adv. Mater.* **1999,** *11*, 579-585.
28. Soler-Illia, G. J. A. A.; Azzaroni, O., Multifunctional hybrids by combining ordered mesoporous materials and macromolecular building blocks, *Chem. Soc. Rev.* **2011,** *40*, 1107-1150.
29. Tagliazucchi, M.; Szleifer, I., Transport mechanisms in nanopores and nanochannels: can we mimic nature?, *Mat. Today* **2015,** *18*, 131-142.
30. Alberti, S.; Soler-Illia, G. J. A. A.; Azzaroni, O., Gated supramolecular chemistry in hybrid mesoporous silica nanoarchitectures: controlled delivery and molecular transport in response to chemical, physical and biological stimuli, *Chem. Commun.* **2015,** *51*, 6050-6075.
31. Travitzky, N.; Windsheimer, H.; Fey, T.; Greil, P., Preceramic Paper-Derived Ceramics, *J. Am. Ceram. Soc.* **2008,** *91*, 3477-3492.
32. Yameen, B.; Ali, M.; Neumann, R.; Ensinger, W.; Knoll, W.; Azzaroni, O., Ionic Transport Through Single Solid-State Nanopores Controlled with Thermally Nanoactuated Macromolecular Gates, *Small* **2009,** *5*, 1287-1291.
33. Ma, Y.; Xue, S.; Hsu, S. C.; Yeh, L. H.; Qian, S.; Tan, H., Programmable ionic conductance in a pH-regulated gated nanochannel, *Phys. Chem. Chem. Phys.* **2014,** *16*, 20138-20146.

34. Calvo, A.; Yameen, B.; Williams, F. J.; Soler-Illia, G. J. A. A.; Azzaroni, O., Mesoporous Films and Polymer Brushes Helping Each Other To Modulate Ionic Transport in Nanoconfined Environments. An Interesting Example of Synergism in Functional Hybrid Assemblies, *J. Am. Chem. Soc.* **2009,** *131*, 10866-10868.
35. Alexander, S.; Morrow, L.; Lord, A. M.; Dunill, C. W.; Barron, A. R., pH-responsive oxtylamine coupling modification of carboxylated aluminium oxide surfaces, *J. Mater. Chem. A.* **2015,** *3*, 10052-10059.
36. Brunsen, A.; Diaz, C.; Pietrasanta, L. I.; Yameen, B.; Ceolin, M.; Soler-Illia, G. J. A. A.; Azzaroni, O., Proton and Calcium-Gated Ionic Mesochannels: Phosphate-Bearing Polymer Brushes Hosted in Mesoporous Thin Films As Biomimetic Interfacial Architectures, *Langmuir* **2012,** *28*, 3583-3592.
37. Shang, Y. L.; Zhang, Y.; P., L.; Kong, X.-Y.; Liu, W.; Xiao, K.; Xie, G.; Tian, Y.; Wen, L.; Jiang, L., DNAzyme tunable lead(II) gating based on ion-track etched conical nanochannels, *Chem. Commun.* **2015,** *51*, 5979-5981.
38. Siwy, Z. S.; Howorka, S., Engineered voltage-responsive nanopores, *Chem. Soc. Rev.* **2010,** *39*, 1115-1132.
39. Seifert, A.; Gopfrich, K.; Burns, J. R.; Fertig, N.; Keyser, U. F., Bilayer-Spanning DNA Nanopores with Voltage-Switching between Open and Closed State, *ACS Nano* **2015,** *9*, 1117-1126.
40. Powell, M. R.; Cleary, L.; Davenport, M.; Shea, K. J.; Siwy, Z., Electric-field-induced wetting and dewetting in single hydrophobic nanopores, *Nat. Nanotechnol.* **2011,** *6*, 798-802.
41. Brunsen, A.; Cui, J.; Ceolín, M.; Campo, A. d.; Soler-Illia, G. J. J. A.; Azzaroni, O., Light-activated gating and permselectivity in interfacial architectures combining “caged” polymer brushes and mesoporous thin films, *Chem. Commun.* **2012,** *48*, 1422-1424.
42. Vlassiouk, I.; Park, C. D.; Vail, S. A.; Gust, D.; Smirnov, S., Control of nanopore wetting by a photochromic spiropyran: A light-controlled valve and electrical switch, *Nano Lett.* **2006,** *6*, 1013-1017.
43. Wang, G.; Bohaty, A. K.; Zharov, I.; White, H. S., Photon Gated Transport at the Glass Nanopore Electrode, *J. Am. Chem. Soc.* **2006,** *128*, 13553-13558.
44. Husseman, M.; Malmström, E. E.; McNamara, M.; Mate, M.; Mecerreyes, D.; Benoit, D. G.; Hedrick, J. L.; Mansky, P.; Huang, E.; Russell, T. P.; Hawker, C. J., Controlled synthesis of polymer brushes by "Living" free radical polymerization techniques, *Macromolecules* **1999,** *32*, 1424-1431.
45. Mazurowski, M.; Gallei, M.; Li, J. Y.; Didzoleit, H.; Stuhn, B.; Rehahn, M., Redox-Responsive Polymer Brushes Grafted from Polystyrene Nanoparticles by Means of Surface Initiated Atom Transfer Radical Polymerization, *Macromolecules* **2012,** *45*, 8970-8981.
46. Metz, G.; Wu, X. L.; Smith, S. O., Ramped-Amplitude Cross Polarization in Magic-Angle-Spinning NMR, *J. Magn. Reson. A* **1994,** *110*, 219-227.
47. Bennett, A. E.; Rienstra, C. M.; Auger, M.; Lakshmi, K. V.; Griffin, R. G., Heteronuclear decoupling in rotating solids, *J. Chem. Phys.* **1995,** *103*, 6951-6958.
48. Koga, H.; Kitaoka, T.; Isogai, A., Chemically-Modified Cellulose Paper as a Microstructured Catalytic Reactor, *Molecules* **2015,** *20*, 1495-1508.
49. Innocenzi, P., Infrared spectroscopy of sol–gel derived silica-based films: a spectra-microstructure overview, *J. Non-Cryst. Solids* **2003,** *316*, 309-319.
50. Gruenberg, A.; Xu, Y. P.; Breitzke, H.; Buntkowsky, G., Solid-State NMR Characterization of Wilkinson’s Catalyst Immobilized in Mesoporous SBA-3 Silica, *Chem. Eur. J.* **2010,** *16*, 6993-6998.
51. Weng, X.; Bao, Z.; Xing, H.; Zhang, Z.; Yang, Q.; Su, B.; Yang, Y.; Ren, Q., Synthesis and characterization of cellulose 3,5-dimethylphenylcarbamate silica hybrid spheres for enantioseparation of chiral β-blockers, *J. Chromatogr. A* **2013,** *1321*, 38-47.
52. Sequeira, S.; Evtuguin, D. V.; Portugal, I.; Esculcas, A. P., Synthesis and Characterization of Cellulose Hybrids Obtained Heteropoly Acid Catalysed Sol–Gel Process, *Mater. Sci. Engin. C* **2007,** *27*, 172-179.
53. Weng, X. L.; Bao, Z. B.; Zhang, Z. G.; Su, B. G.; Xing, H. B.; Yang, Q. W.; Yang, Y. W.; Ren, Q. L., Preparation of Porous Cellulose 3,5-Dimethylphenylcarbamate Hybrid Organosilica Particles for Chromatographic Applications, *J. Mater. Chem. B* **2015,** *3*, 620-628.

54. Ikai, T.; Yamamoto, C.; Kamigaito, M.; Okamoto, Y., Efficient Immobilization of Cellulose Phenylcarbamate Bearing Alkoxysilyl Group onto Silica Gel by Intermolecular Polycondensation and Its Chiral Recognition, *Chem. Lett.* **2006,** *35*, 1250-1251.
55. Ikai, T.; Yamamoto, C.; Kamigaito, M.; Okamoto, Y., Organic-inorganic hybrid materials for efficient enantioseparation using cellulose 3,5-dimethylphenylcarbamate and tetraethyl orthosilicate, *Chem. Asian J.* **2008,** *3*, 1494-1499.
56. Zhang, X.; Wu, W.; Wang, J.; Liu, C., Effects of sol aging on mesoporous silica thin films organization, *Thin Solid Films* **2007,** *515*, 8376-8380.
57. Mantanis, G. I.; Young, R. A.; Rowell, R. M., Swelling of compressed cellulose fiber webs in organic liquids, *Cellulose* **1995,** *2*, 1-22.

Table of Contents artwork